Superposition model analysis from polarized electronic absorption spectra of Co^{2+} in trigonally distorted octahedra in brucite-type $Co(OH)_2$

2001 J. Phys.: Condens. Matter 13 7353

(http://iopscience.iop.org/0953-8984/13/33/315)

INSTITUTE OF PHYSICS PUBLISHING JOURNAL OF PHYSICS: CONDENSED MATTER

J. Phys.: Condens. Matter **13** (2001) 7353–7361 PII: S0953-8984(01)24143-5

Superposition model analysis from polarized electronic absorption spectra of Co^{2+} in trigonally distorted octahedra in brucite-type $Co(OH)_2$

M Andrut and M Wildner

Institut für Mineralogie und Kristallographie, Universität Wien, Geozentrum, Althanstraße 14, A-1090 Wien, Austria

E-mail: manfred.wildner@univie.ac.at

Received 20 April 2001, in final form 12 June 2001
Published 2 August 2001
Online at stacks.iop.org/JPhysCM/13/7353

Abstract

Polarized electronic absorption spectra of Co^{2+} in trigonally compressed octahedra in brucite-type $Co(OH)_2$ have been measured at 290 and 90 K by microscope-spectrometric techniques and analysed in terms of the superposition model (SM) of crystal fields. The resulting SM and interelectronic repulsion parameters are $\overline{B}_4 = 5260$, $\overline{B}_2 = 4920$, Racah B = 825, Racah C = 3550 cm^{-1} at 290 K and $\overline{B}_4 = 5320$, $\overline{B}_2 = 3900$, Racah B = 830, Racah C = 3500 cm^{-1} at 90 K ($R_0 = 2.1115$ Å; fixed exponential and spin–orbit parameters $t_4 = 5$, $t_2 = 3$, $\zeta = 500$ cm^{-1}). Together with a recent SM analysis of $Li_2Co_3(SeO_3)_4$, the $\overline{B}_k$ refined for $Co(OH)_2$ further confine the magnitude of the hitherto unknown 'correct' SM parameters of Co^{2+} for future application to structurally and/or chemically less well defined systems.

1. Introduction

The superposition model (SM) of crystal fields was originally developed to separate the geometrical and physical information inherent in crystal field parameters. It is based on the assumption that the crystal field can be expressed as the sum of the axially symmetric contributions of all i nearest-neighbour ligands of a transition metal ion. The crystal field parameters B_{kq} can then be obtained from

$$B_{kq} = \sum_i \overline{B}_k(R_0)\left(\frac{R_0}{R_i}\right)^{t_k} K_{kq}(\Theta_i, \Phi_i)$$

where $\overline{B}_k$ are the intrinsic parameters (related to a reference metal–ligand distance R_0) and t_k are the power law exponent parameters, both for each rank k of the crystal field; R_i are the individual metal–ligand distances; and $K_{kq}(\Theta_i, \Phi_i)$ are the coordination factors calculated from the angular polar coordinates of the ligands. For comprehensive reviews on the SM, the

reader is referred to Newman (1971) and Newman and Ng (1989), explicit expressions for $K_{kq}(\Theta_i, \Phi_i)$ are given, for example, by Rudowicz (1987).

Since its introduction by Bradbury and Newman (1967), the SM has been applied with considerable success to the analysis of lanthanide crystal fields. In contrast, to date SM investigations on d-block transition elements are scarce. Hence, the necessary intrinsic and power law exponent parameters for application to systems containing d-block elements, for example in geosciences, are practically missing or were obtained from natural, dilute phases, where the local structure around the particular transition ion is not exactly known (e.g. Cr^{3+} in alumosilicates (Qin *et al* 1994, Yeung *et al* 1994)). In order to provide reliable SM parameters of $3d^n$ elements for future applications in geosciences, we started to investigate inorganic model compounds, i.e. pure synthetic endmember phases, where the (local) structure is precisely known from concurrent or recent structural investigations. The first SM parameter set for Co^{2+} was extracted from polarized electronic absorption spectra of $Li_2Co_3(SeO_3)_4$, which is characterized by strong bond length and angle distortions of its CoO_6 polyhedra with low symmetries C_1 and C_i (Wildner and Andrut 1999). In the present paper we report temperature dependent polarized spectra and SM analyses of brucite-type $Co(OH)_2$, where the Co^{2+} ions occupy a high-symmetry site (D_{3d}) within a compressed hexagonal close packing of oxygen atoms, aiming at a further confinement of the 'correct' global SM parameters for Co^{2+}.

2. Relevant structure details

$Co(OH)_2$ crystallizes in the structure type of brucite, $Mg(OH)_2$, in space group $P\bar{3}m1$ (D^3_{3d}). This structure type is characterized by the formation of layers parallel to (0001), built up from edge sharing $Me^{2+}(OH)_6$ octahedra, which are interlinked by weak hydrogen bonds along [0001]. The Me^{2+} cation occupies the $1a$ site of $P\bar{3}m1$ with point symmetry $\bar{3}m$ (D_{3d}), oxygen occupies a $2d$ position (point symmetry $3m$, C_{3v}) and the H (or D) atoms are also located on a $2d$ site (at least at ambient pressure). The MeO_6 octahedron is generally compressed along its trigonal axis, thus increasing the $\bar{3}$–Me–O angle Θ above the ideal octahedral value of 54.74°.

The crystal structure of $Co(OH)_2$ at room temperature was recently refined by Pertlik (1999) from single crystal x-ray data. The respective results for the $Co(OH)_6$ octahedron are shown in figure 1. In order to obtain unbiased structural input values for the SM calculations based on the low-temperature spectra, we refined the structure of $Co(OH)_2$ at 90 K from single-crystal x-ray CCD data, showing that the octahedral shape changes only slightly towards shorter Co–O bond lengths and marginally increased the octahedral compression. Relevant data are included in figure 1, further details of the low-temperature structure investigation can be obtained from the authors upon request.

It is noteworthy that Rietveld refinements of $Co(OD)_2$ from neutron powder data at room temperature were also recently reported by Parise *et al* (1998) and Mockenhaupt *et al* (1998). Both indicate that at ambient pressure the axiality of the crystal field around Co^{2+} is obeyed also in regard to the position of the H(D) atom. According to Parise *et al* (1998), a split-site model where the deuterium shifts from site $2d$ to $6i$ (symmetry m, C_s) is preferable only at pressures above 8 GPa. Concerning the geometry of the CoO_6 octahedron, the structural results by Parise *et al* (1998) (Co–O = 2.115 Å, $\bar{3}$–Co–O = 60.4°) are in perfect agreement with Pertlik's (1999) data, whereas the refinement by Mockenhaupt *et al* (1998) yielded a significantly shorter Co–O distance (2.083 Å) and a stronger octahedral compression ($\bar{3}$–Co–O = 61.7°). Given the much higher reliability of the single-crystal x-ray data in regard to the CoO_6 polyhedral shape, as well as the congruent results of the neutron Rietveld analysis by Parise *et al* (1998), all our further calculations refer to the x-ray results given in figure 1.

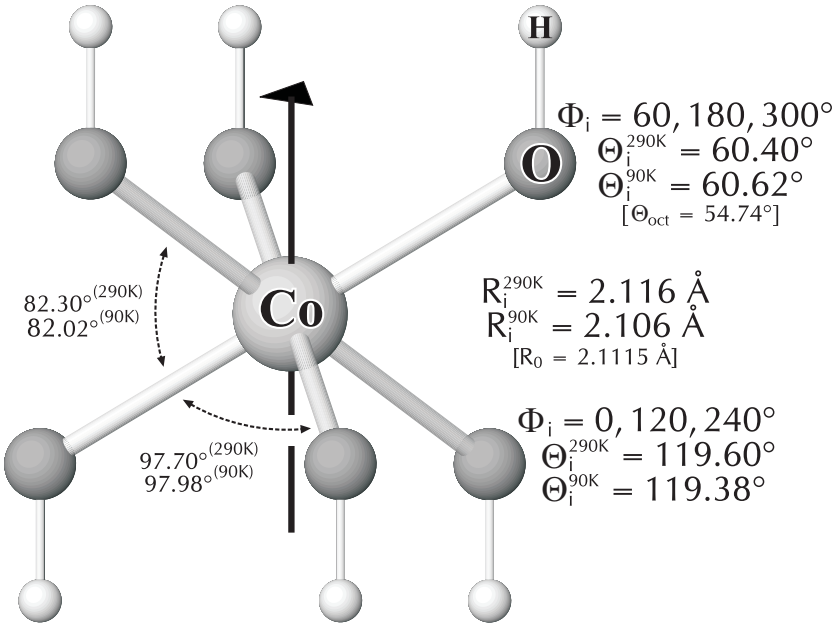

Figure 1. Structural details of the $Co(OH)_6$ polyhedron in brucite-type $Co(OH)_2$ at 290 K (Pertlik 1999), 90 K (this paper) and polar coordinates of the oxygen atoms used in the SM calculations.

3. Experiment

Single crystals of $Co(OH)_2$ suitable for the present investigations were synthesized at our laboratory by Pertlik (1999) under low-hydrothermal conditions. The pink pleochroic crystals (orange to reddish pink in transmission) exhibit a platy habit (dominant form (0001)) at a maximal size of 1.0 × 0.2 mm, requiring the application of microscope-spectrometric techniques. Hence, polarized electronic absorption spectra were measured in the range 35 000–5000 cm^{-1} at ambient and 31 000–5000 cm^{-1} at liquid nitrogen temperatures on an IRscopeII mirror-optics microscope attached to a Bruker IFS66v/s FT-spectrometer. A calcite glan-prism was used as polarizer. The low-temperature measurements were done with a Linkham THM600IR cooling stage. Appropriate combinations of light sources (globar, tungsten lamp, Xe lamp), beam splitters (KBr, quartz) and detectors (MCT, Si diode, Ge diode, GaP diode) were used in different spectral regions. The local resolution was 60 μm in each case, the spectral resolution was 10 cm^{-1} in the UV–VIS and 1 cm^{-1} in the NIR regions. Spectra were averaged over 1024 scans in the UV–VIS range and 256 scans in the NIR range. The phase correction mode of the interferogram was performed with a procedure after Mertz (e.g. Griffiths and de Haseth 1986). A Norton–Beer weak mode was chosen as the apodization function. According to the crystal symmetry, polarized spectra had to be recorded with the electric light vector parallel and perpendicular to the $\bar{3}$-axis, i.e. parallel to the optic axes E and O, respectively. Therefore, a crystal slab containing the trigonal axis was prepared by grinding and polishing an oriented crystal from both sides to a thickness of 45 μm. For comparison, the O-spectrum was also recorded on the (0001) face of an unprepared crystal; since both O-spectra are practically identical, the contribution of electronic quadrupole transitions seems to be negligible. The various partial spectra were finally merged and are displayed in figure 2 as linear absorption coefficient α against wavenumber ν. The observed transition energies

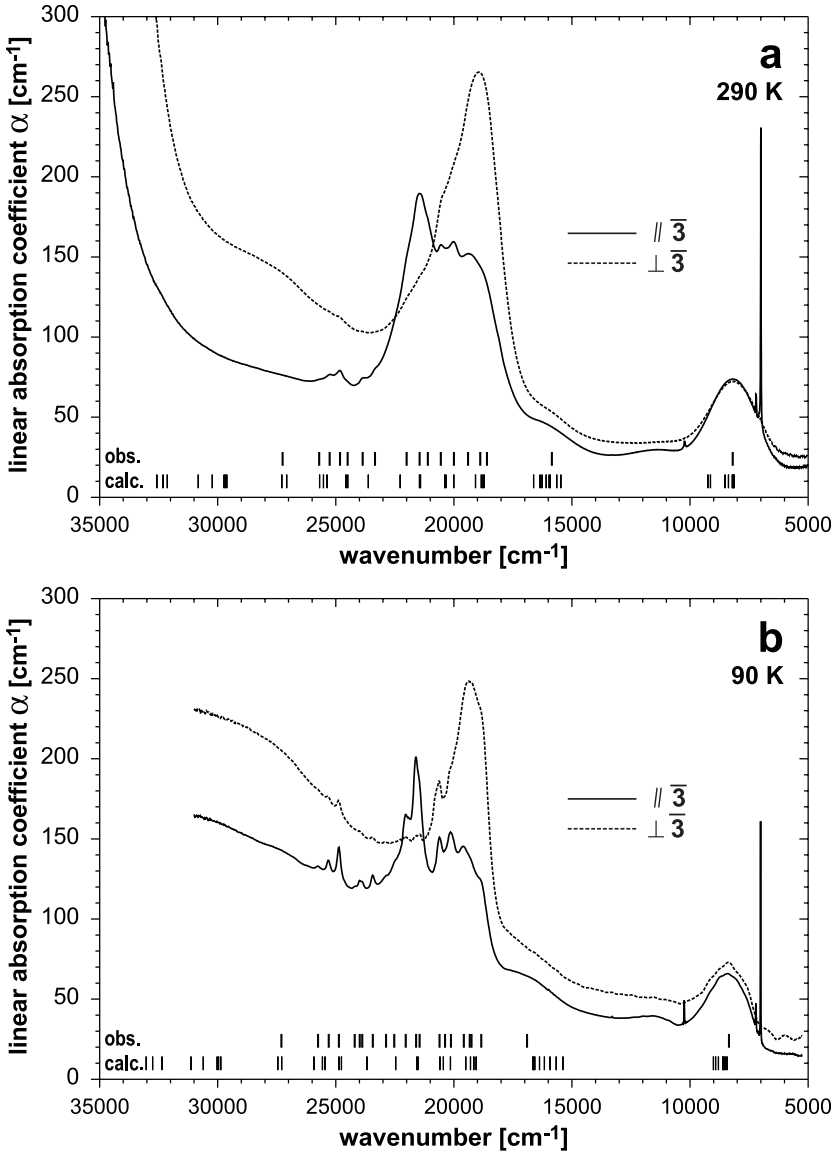

Figure 2. Polarized electronic absorption spectra of $Co(OH)_2$ at (a) 290 K and (b) 90 K. The bold and normal line marks represent the observed and calculated transition energies, respectively. Sharp lines in the NIR region are overtones of the OH stretching vibration.

were extracted by visual inspection and/or by Gaussian peak deconvolution procedures and are plotted as bold line marks in figure 2, numerical values are included in figure 3.

Crystal field calculations were performed using the HCFLDN2-module of the crystal field analysis computer package by Yeung (Chang *et al* 1994); some additional calculations were also carried out with the program TETRIG (Wildner 1996a). Supplementary programs developed by the authors (Wildner and Andrut, unpublished) were used (i) for the transformation of atomic to polyhedral polar coordinates; (ii) for the systematic variation of the SM parameters and of Racah B, and for the corresponding communication with the

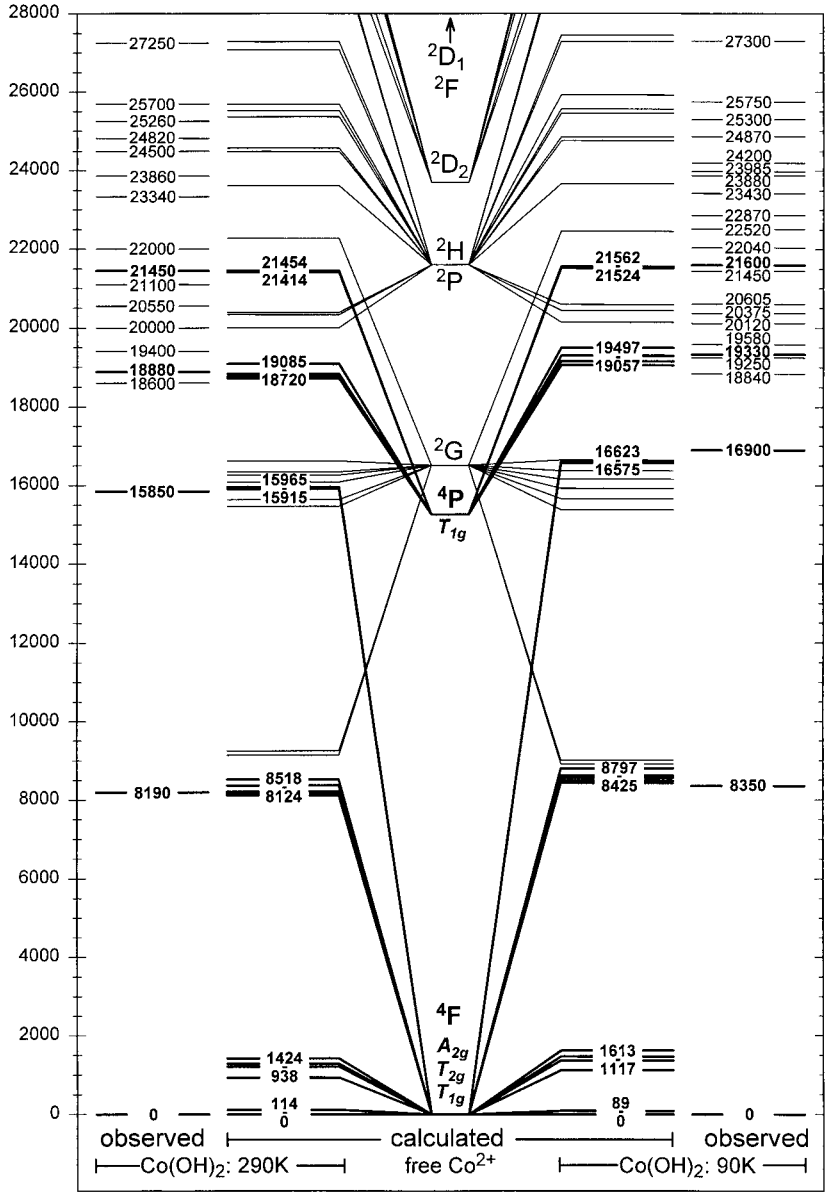

Figure 3. Graphical representation of the observed and calculated energy levels in $Co(OH)_2$ up to 28 000 cm^{-1}. Parental free ion term labels and quartet split labels for O_h symmetry are given. All bold lines, numbers and labels refer to spin-allowed, normal to spin-forbidden levels. Ranges of calculated spin-allowed energies are included, a complete and detailed listing of all spin–orbit components can be obtained from the authors upon request.

HCFLDN2 program; (iii) for the SM calculation itself, giving values for the B_{kq}'s; and (iv) for the interpretation of the HCFLDN2 output results in terms of a reliability index for the agreement of calculated and observed spin-allowed transition energies. Racah C was subsequently estimated from the positions of some safely identified spin-forbidden transitions.

According to the point symmetry of the CoO_6 octahedron discussed above, the electronic z-axis of the crystal field was chosen parallel to the crystallographic $\overline{3}$-axis, leading to the polar coordinates given in figure 1. Due to the fact that there exists only one reliable set of SM parameters $\overline{B}_k$ and t_k for the Co^{2+} cation up to now (Wildner and Andrut 1999), we decided to vary the intrinsic $\overline{B}_k$ parameters and Racah B over a wide range in order to avoid wrong local minima in the fitting process. The reference metal–ligand distance R_0 was set to 2.1115 Å, the overall mean bond length of Co^{2+} in octahedral coordination to oxygen (Wildner 1992). Due to the high point symmetry of the CoO_6 octahedron with six equal Co–O bonds, the power law exponent parameters t_k could not be refined. Moreover, since $R_i \approx R_0$, the particular values of t_k have only marginal influence on the calculations and were hence fixed at $t_4 = 5$ and $t_2 = 3$, values derived from purely electrostatic considerations (Newman and Ng 1989). While on the one hand the calculational effort was notably reduced by the high D_{3d} site symmetry and the appropriate alignment of the local axes, resulting in all imaginary parts of the B_{kq}'s being zero; on the other hand preliminary calculations showed that spin–orbit coupling effects could not be neglected. In order to keep the calculation time at a reasonable level, the spin–orbit coupling coefficient ζ was not included in the systematic parameter refinement, but was estimated in the preliminary calculations to be $\zeta \approx 500\ cm^{-1}$, i.e. ~90% of the Co^{2+} free ion value.

4. Results and discussion

4.1. Electronic absorption spectra

The gross spectral features of the electronic absorption spectra of $Co(OH)_2$ shown in figure 2 are typical for Co^{2+} ions in octahedral coordination by oxygen ligands. Two main regions of absorption around 8200 cm^{-1} and 18 000–22 000 cm^{-1} are correlated predominantly with spin-allowed d–d transitions from the ground state $^4T_{1g}(^4F)$ to the $^4T_{2g}(^4F)$ and $^4T_{1g}(^4P)$ states in O_h symmetry. A weak and broad band at ~16 000 cm^{-1} is attributed to the spin-allowed $^4T_{1g}(^4F) \rightarrow {}^4A_{2g}(^4F)$ transition which in the strong field limit represents an electronically forbidden two-electron jump ($t_{2g}^5 e_g^2 \rightarrow t_{2g}^3 e_g^4$) with low probability (e.g. Lever 1984). The strong splitting and structure of the intense VIS band system indicates on one hand the substantial trigonal perturbation of the octahedral crystal field, on the other hand the significant contribution of intensity enhanced spin-forbidden quartet → doublet transitions and further splitting due to spin–orbit coupling.

Upon symmetry reduction from O_h to the actual symmetry D_{3d}, triply degenerate states split into $A_{2g} + E_g$ (T_{1g}) or $A_{1g} + E_g$ (T_{2g}), while A_{2g} remains A_{2g}. As a consequence of the centric field symmetry around Co^{2+}, d–d dipole transitions are in principle Laporte forbidden and may only gain intensity by coupling with acentric octahedral vibrational modes. Hence, for the interpretation of the polarization behaviour, symmetry selection rules for the acentric trigonal point groups were checked for their applicability to the $Co(OH)_2$ spectra. The polarization behaviour can then be reasonably explained by C_3 symmetry selection rules with an A ground state, allowing A → A transitions parallel, and A → E transitions perpendicular to the trigonal axis. The A ground state is also in principal agreement with the octahedral compression along the trigonal axis.

Since the $T_{2g}(F)$ band in the NIR is obviously not split by the trigonal field and the weak band around 16 000 cm^{-1} is singly degenerate, their assignment, as outlined above, is clear cut. Nearby spin-forbidden levels with a parental ^2G term are not observed. Contrary to the $^4T_{2g}(^4F)$ level, the spin-allowed $^4T_{1g}(^4P)$ state is strongly split into components at 18 900 and 21 450 cm^{-1} which, according to the C_3 symmetry selection rules, represent the E and A split levels, respectively. Weaker and comparatively sharp spectral features around 20 000 cm^{-1}

can be assigned to split levels of the spin-forbidden $^2T_{1g}$ state with a parental ^2P term, which gain up to ∼25% quartet character (up to 35% at 90 K) from the nearby spin-allowed levels. A further spectral feature in the high-energy wing of the spin-allowed band at 22 000 cm^{-1}, especially visible in the 90 K spectra, most probably represents the $^2A_{1g}$ level with predominant spin-forbidden ^2G character. Further weak bands observed between ∼23 000 and 27 000 cm^{-1} all arise from the ^2H free ion term with admixture of other spin-forbidden states (^2G, $^2D_{1,2}$, ^2P) and at most ∼1% quartet contribution at around 25 000 cm^{-1}. Higher spin-forbidden d–d levels, calculated around 30 000 cm^{-1} (arising from $^2D_2$) and above (^2H, ^2F, $^2D_1$) are not observed, respectively obscured by the onset of the charge-transfer absorption edge which also exhibits a clear polarization dependence.

Upon cooling to liquid nitrogen temperatures, the absorption intensities of the spin-allowed bands decrease, in agreement with their vibronic origin, while some of the spin-forbidden bands are slightly intensified due to a somewhat enhanced quartet admixture. The band widths are generally reduced. For example, at 90 K the integral absorption of the (background-corrected) band system in the VIS spectral region is reduced by more than 45%. As a consequence of the different crystal field dependences of the energy levels and of the various parameter shifts with temperature, the observed blue-shifts of the absorption bands upon cooling range from merely ∼50 cm^{-1} up to ∼1000 cm^{-1} for the $^4T_{1g}(^4F) \rightarrow {}^4A_{2g}(^4F)$ two-electron transition.

Beside electronic transitions, the first, second and at 90 K also the third overtones ($2\nu_{OH}-4\nu_{OH}$) of the OH stretching vibration, strictly polarized parallel to the trigonal axis, are located at 7000.9 + 7199.8 and 10 229.4 cm^{-1} (290 K, FWHH 25–38 cm^{-1}), respectively at 7012.5 + 7211.2, 10 244.6 and 13 294.0 cm^{-1} (90 K, FWHH 20–31 cm^{-1}). Mockenhaupt *et al* (1998) observed the respective fundamental vibrational modes in powder spectra at 3627 cm^{-1} (295 K) and 3633 cm^{-1} (90 K). In addition to the x-ray and neutron diffraction data discussed above, the perfect polarization of the OH stretching overtones confirms the effective axiality of the crystal field in $Co(OH)_2$.

4.2. Crystal field SM calculations

In the fitting of the intrinsic SM parameters ($\overline{B}_4$, $\overline{B}_2$) and free ion parameters (Racah B and Racah C), the best agreement of observed and calculated energy levels was achieved with the following parameter sets: $\overline{B}_4 = 5260$, $\overline{B}_2 = 4920$, Racah B = 825, Racah C = 3550 cm^{-1} for 290 K and $\overline{B}_4 = 5320$, $\overline{B}_2 = 3900$, Racah B = 830, Racah C = 3500 cm^{-1} for 90 K, both sets with fixed exponential and spin–orbit parameters $t_4 = 5$, $t_2 = 3$, $\zeta = 500$ cm^{-1}, and based on $R_0 = 2.1115$ Å. Table 1 summarizes these parameters as well as non-zero B_{kq}'s, rotational invariants s_k (Leavitt 1982, Yeung and Newman 1985), and the resulting cubic crystal field strengths Dq_{cub}. Calculated energy levels are depicted in figure 3, including ranges of numerical values for the predominant spin-allowed transitions. A complete and detailed listing of all spin–orbit components can be obtained from the authors upon request.

At first, it has to be noted that the general expectation $\overline{B}_4 < \overline{B}_2$ (Yeung and Newman 1986) is not met for $Co(OH)_2$. However, the magnitudes of the respective $\overline{B}_k$ tolerably comply with the only reliable data set obtained so far for Co^{2+}, namely $\overline{B}_4 = 4740$ cm^{-1} and $\overline{B}_2 = 7000$ cm^{-1} in $Li_2Co_3(SeO_3)_4$, where the exponential parameters could also be refined to $t_4 = 3.1$ and $t_2 = 5.5$ (Wildner and Andrut 1999). A larger discrepancy exists with earlier data extracted from electron paramagnetic resonance spectra of Co^{2+} doped in chloride salts: Edgar (1976) gives $|\overline{B}_4| = 4060$ cm^{-1} and $|\overline{B}_2| = 11\,000$ cm^{-1}, but reports neither exponential parameters nor a reference distance R_0, which makes the $\overline{B}_k$ hardly useful for comparison. The particular difference of the $\overline{B}_4$ parameters in $Co(OH)_2$ and $Li_2Co_3(SeO_3)_4$ can be explained by the fact that the $(OH)^-$ group doubtlessly occupies a higher position in the

Table 1. Summary of crystal field parameters (non-zero B_{kq} in Wybourne notation, intrinsic $\overline{B}_k$, rotational invariants s_k, cubic field strengths Dq_{cub}) and interelectronic repulsion parameters for $Co(OH)_2$ at 290 and 90 K. Values are in cm^{-1} (except t_k, β and Racah C/Racah B).

$Co(OH)_2$	290 K	90 K
B_{20}	−3931	−3274
B_{40}	−8739	−8860
B_{43}	15 010	15 512
$\overline{B}_4$	5260	5320
$\overline{B}_2$	4920	3900
s_4	7652	7886
s_2	1758	1464
Dq_{cub} (from s_4)	835	860
t_4 (fixed)	5	5
t_2 (fixed)	3	3
Racah B	825	830
Racah C	3550	3500
β ($B_0 = 1018$)	0.81	0.82
Racah C/Racah B	4.30	4.22
ζ (fixed)	500	500

spectrochemical series of oxygen based ligands compared with the $(SeO_3)^{2-}$ anion. The low position of the selenite anion has been consistently corroborated for selenites of Co^{2+}, Cr^{3+} and Mn^{4+} (Wildner and Langer 1994a,b, Wildner 1995, 1996b, Wildner and Andrut 1998, 1999), thus explaining the reduced $\overline{B}_4$ in $Li_2Co_3(SeO_3)_4$. The larger difference of the $\overline{B}_2$ in these two compounds, as well as the strong temperature shift of $\overline{B}_2$ and the untypical hierarchy of the $\overline{B}_k$ in $Co(OH)_2$, indicate that the obtained $\overline{B}_2$ should be treated with some caution. Anyhow, it can yet be stated that $\overline{B}_4$ and $\overline{B}_2$ take similar magnitudes for high-spin Co^{2+} in octahedral coordination by oxygen atoms.

Given the high symmetry of the crystal field in $Co(OH)_2$, the obtained SM parameters are directly related to the 'classical' crystal field parameters for trigonal symmetry, i.e. $Dq_{(trig)}$, $D\tau$ and $D\sigma$ (e.g. Ballhausen 1962). The corresponding values are $Dq_{(trig)} = 897\ cm^{-1}$, $D\tau = -182\ cm^{-1}$, $D\sigma = 562\ cm^{-1}$ at 290 K and $Dq_{(trig)} = 927\ cm^{-1}$, $D\tau = -196\ cm^{-1}$, $D\sigma = 468\ cm^{-1}$ at 90 K. The respective cubic crystal field strengths Dq_{cub} are 826 and 851 cm^{-1} (the small differences of Dq_{cub} in table 1, calculated from s_4, is due to the neglect of spin–orbit coupling in the 'classical' evaluation). The $D\tau$ values closely comply with those predicted from the geometrical compression of the CoO_6 octahedron, namely −175 and −187 cm^{-1}, respectively. A similar good agreement in terms of the classical trigonal distortion parameter $D\tau$ was also found for the elongated centric CoO_6 octahedron (symmetry D_{3d}) in $K_2Co(SeO_3)_2$, whereas in the structurally related compounds $K_2Co_2(SeO_3)_3$ and $K_2Co_2(SeO_3)_3 \cdot 2H_2O$, containing octahedral pairs with common faces (octahedral symmetry C_{3v} and C_3, respectively), the deviation of predicted and observed $D\tau$ values strongly increases with octahedral acentricity and approaching Co–Co contacts (Wildner and Langer, 1994a).

The magnitude of the interelectronic repulsion parameters Racah B and Racah C are in a range typical for Co^{2+} cations in oxygen coordination: the nephelauxetic ratio β referring to the free ion value ($B_0 = 1018\ cm^{-1}$, Uylings *et al* 1984) is ∼0.81; the ratio Racah C/Racah B, commonly ranging between 4.1 and 4.6, is 4.30 at 290 K and 4.22 at 90 K. Ludi and Feitknecht (1963) calculated $Dq = 830\ cm^{-1}$ from diffuse reflectance spectra of $Co(OH)_2$, but reported no interelectronic repulsion or other parameters.

5. Conclusions

The present investigation confirms the effective applicability of the SM concept to d-block-element compounds. The magnitudes of the 'correct' SM parameters of Co^{2+} for future application to structurally and/or chemically less well defined systems, for example in geosciences, have been further confined. However, it appears that the specific position of closely related ligands within the spectrochemical series affects the intrinsic $\overline{B}_k$. Therefore, especially for mixed-ligand coordinations, it might be worthwhile to apply some empirical correction factor for the ligand type in the SM equation—resembling the f-factor formerly introduced by Jørgensen (1962)—instead of refining different SM parameter sets for each ligand type.

Acknowledgments

Thanks are due to F Pertlik (Vienna) for providing single crystals of $Co(OH)_2$, to A Wagner (Vienna) for the careful sample preparation, and to Y Y Yeung (Hong Kong) for a copy of his crystal field analysis computer package. M A gratefully acknowledges financial support by a research fellowship from the *Fonds zur Förderung der wissenschaftlichen Forschung*, Austria (project P13976-CHE).

References

Ballhausen C J 1962 *Introduction to Ligand Field Theory* (New York: McGraw-Hill)
Bradbury M I and Newman D J 1967 *Chem. Phys. Lett.* **1** 44–5
Chang Y M, Rudowicz C and Yeung Y Y 1994 *Comput. Phys.* **8** 583–8
Edgar A 1976 *J. Phys. C: Solid State Phys.* **9** 4303–14
Griffiths P R and de Haseth J A 1986 *Fourier Transform Infrared Spectroscopy* (New York: Wiley)
Jørgensen C K 1962 *Absorption Spectra and Chemical Bonding in Complexes* (Oxford: Pergamon)
Leavitt R P 1982 *J. Chem. Phys.* **77** 1661–3
Lever A B P 1984 *Inorganic Electronic Spectroscopy* 2nd edn (Amsterdam: Elsevier)
Ludi A and Feitknecht W 1963 *Helv. Chim. Acta* **46** 2226–38
Mockenhaupt C, Zeiske T and Lutz H D 1998 *J. Mol. Struct.* **443** 191–6
Newman D J 1971 *Adv. Phys.* **20** 197–256
Newman D J and Ng B 1989 *Rep. Prog. Phys.* **52** 699–763
Parise J B, Theroux B, Li R, Loveday J S, Marshall W G and Klotz S 1998 *Phys. Chem. Minerals* **25** 130–7
Pertlik F 1999 *Monatsh. Chem.* **130** 1083–8
Qin J, Rudowicz C, Chang Y M and Yeung Y Y 1994 *Phys. Chem. Minerals* **21** 532–8
Rudowicz C 1987 *J. Phys. C: Solid State Phys.* **20** 6033–7
Uylings P H M, Raassen A J J and Wyart J F 1984 *J. Phys. B: At. Mol. Phys.* **17** 4103–26
Wildner M 1992 *Z. Kristallogr.* **202** 51–70
——1995 *J. Solid State Chem.* **115** 360–7
——1996a *Abstracts EMSMM'96 (Kiev)*
——1996b *J. Solid State Chem.* **124** 143–50
Wildner M and Andrut M 1998 *J. Solid State Chem.* **135** 70–7
——1999 *Z. Kristallogr.* **214** 216–22
Wildner M and Langer K 1994a *Phys. Chem. Minerals* **20** 460–8
——1994b *Phys. Chem. Minerals* **21** 294–8
Yeung Y Y and Newman D J 1985 *J. Chem. Phys.* **82** 3747–52
——1986 *Phys. Rev.* B **34** 2258–65
Yeung Y Y, Qin J, Chang Y M and Rudowicz C 1994 *Phys. Chem. Minerals* **21** 526–31